Icarus 000 (2017) 1–12

Contents lists available at ScienceDirect

Icarus

journal homepage: www.elsevier.com/locate/icarus

Mineralogical mapping of Coniraya quadrangle of the dwarf planet Ceres

A. Raponi[a,*], F.G. Carrozzo[a], F. Zambon[a], M.C. De Sanctis[a], M. Ciarniello[a], A. Frigeri[a], E. Ammannito[b], F. Tosi[a], J.-Ph. Combe[c], A. Longobardo[a], E. Palomba[a], C.M. Pieters[d], C.A. Raymond[e], C.T. Russell[f]

[a] INAF-IAPS Istituto di Astrofisica e Planetologia Spaziali, Via del Fosso del Cavaliere, 100, I-00133 Rome, Italy
[b] Italian Space Agency (ASI), Via del Politecnico snc, I-00133 Rome, Italy
[c] Bear Fight Institute, 22, Fiddler's Road, P.O. Box 667, Winthrop, WA 98862, USA
[d] Department of Earth, Environmental and Planetary Sciences, Brown University, 324 Brook Street, Providence, RI 02912, USA
[e] NASA/Jet Propulsion Laboratory and California Institute of Technology, 4800 Oak Grove Drive, Pasadena, CA 91109, USA
[f] Institute of Geophysics and Planetary Physics, University of California at Los Angeles, 3845 Slichter Hall, 603 Charles E. Young Drive, East, Los Angeles, CA 90095-1567, USA

ARTICLE INFO

Article history:
Received 28 April 2017
Revised 15 September 2017
Accepted 12 October 2017
Available online xxx

ABSTRACT

Ceres has been explored by NASA/Dawn spacecraft, which allowed for the discovery of the main mineralogical and compositional characteristics of Ceres' surface. Here, we use mainly data from the Visible and InfraRed imaging spectrometer (VIR) in order to investigate the main spectral characteristics of the quadrangle Ac-H-2 Coniraya, one of the 15 quads in which Ceres' surface has been divided. Coniraya quadrangle is characterized by the presence of mostly highly degraded impact craters of diameters between 50 and 200 km and clusters of small to midsize impact craters. Although the composition over the quadrangle appears to be quite uniform, significant differences have been detected between different craters by spectral parameters analysis and spectral modeling. Ernutet crater presents two regions with very peculiar band at 3.4 μm, typical of organics aliphatic material. One region result to be correlated with larger amount of carbonates, the other region does not present such correlation. Ikapati crater shows strong absorption bands at 4.0 μm, indicating the presence of Na-carbonates in the floor and ejecta. Ikapati, Gaue and other craters present smaller spectral features of NH_4 and/or OH stretching, suggesting a volatile depletion process induced by the heating of the impact event.

1. Introduction

NASA's Dawn spacecraft arrived at dwarf planet 1-Ceres on March 6, 2015, with its scientific payload: the Visible and near-InfraRed imaging spectrometer (VIR) (De Sanctis et al., 2011), the Gamma Ray and Neutron Detector (GRaND) (Prettyman et al., 2011), and the Framing Camera (FC) (Sierks et al., 2011), along with the radio science package (Konopliv et al., 2011).

Here, we use data returned by VIR and FC instruments in order to study the mineralogical composition of the quadrangle Ac-H-2 'Coniraya' (21–66 °N and 0–90 °E), which is one of four quadrangles in Ceres' northern hemisphere.

Ceres' surface shows ubiquitous absorption bands at 2.7 μm (OH stretching in Mg-phyllosilicates) and 3.1 μm related NH4-phyllosilicates, respectively (De Sanctis et al., 2015; Ammannito et al., 2016).

The thermally-corrected reflectance spectrum of Ceres shows several distinct absorption bands at 3.3–3.5, and 3.95 μm, related to the presence of Mg-carbonates and NH_4-phyllosilicates (De Sanctis et al., 2015).

Although spectral properties of Ceres' surface are quite uniform, there are some peculiar areas where significant differences have been detected in spectral parameters such as slopes, albedo, band depths and band centers. The case that stands out above the surrounding terrains are the bright areas ("Ceralia and Vinalia faculae") in the Occator crater (De Sanctis et al., 2016; Raponi et al., 2017; Longobardo et al., 2017), where the albedo is 5–10 times higher than the average surface. The OH feature in these faculae is shifted from 2.72 to 2.76 μm, indicating the presence of Al-phyllosilicates, while the carbonate features are shifted from 3.95 to 4.0 μm with increasing band depth, suggesting a large abundance of Na-carbonates (De Sanctis et al., 2016). Additionally to

* Corresponding author.
E-mail address: andrea.raponi@iaps.inaf.it (A. Raponi).

https://doi.org/10.1016/j.icarus.2017.10.023
0019-1035/

the Occator crater, other areas show a signature of Na-carbonates (Carrozzo et al. 2017), e.g., Ikapati crater, located in the 'Coniraya' quadrangle, which is part of the analysis done in the present work.

Knowledge of the mineralogy of Ceres has been enriched by the discovery of organic material mainly in the form of aliphatic material (De Sanctis et al. 2017) near the Ernutet crater (latitude ~53°N, longitude 45.5°E, diameter 53.4 km), contained in Coniraya quadrangle.

Oxo crater is another interesting region, which the Coniraya quadrangle shares with the Ac-H-5 'Fejokoo' crater, but which is mostly located in the latter. It is a fresh crater where a large amount of water ice has been detected (Combe et al., 2016; Raponi et al., 2016; Combe et al., 2017). Moreover, it is the second brightest feature on Ceres after the bright material of the Occator crater. Water ice was detected near the southern rim and corresponds to the high albedo materials on the floor of the crater (Combe et al., 2016). The water ice location is entirely in the 'Fejokoo' quadrangle. We refer to Combe et al. (2017), and Singh et al. (2017) for further details about this crater.

In Section 2, we present the dataset and the methodology used to perform the spectral analysis. In Section 3, the thermal emission removal, relevant for the discussion of the spectra in the thermal emission range, is described. In Section 4, we give a general view of the quadrangle, discussing the spectral parameters, such as band centers, band depth, spectral slope and albedo. In Section 5, we present a quantitative analysis of abundances of the main minerals identified as component of surface materials, by means of the Hapke radiative transfer model. The main findings are discussed in Section 6, under the general context of Ceres' surface.

2. Data analysis description

The present work uses the dataset acquired by VIR, the mapping spectrometer of the Dawn mission (Russell and Raymond, 2011; De Sanctis et al., 2011). Images provided by the Dawn Framing Camera (Sierks et al., 2011) are also used for context and morphological analysis.

VIR is an imaging spectrometer operating in two channels: the visible channel, ranging between 0.25–1.05 μm, and the infrared channel, between 1.0–5.1 μm. VIR is capable of high spatial (IFOV = 250 μrad/pixel, FOV = 64 × 64 mrad) and spectral ($\Delta\lambda$VIS = 1.8 nm/band; $\Delta\lambda$IR = 9.8 nm/band) performances, allowing for the identification of spectral features in order to derive the composition, structure of the surface, and thermal emission.

VIR acquired data of Ceres during all of the mission phases: Survey (spacecraft altitude 4350 km), High Altitude Mapping Orbit (HAMO) (spacecraft altitude 1450 km) and Low Altitude Mapping Orbit (LAMO) (spacecraft altitude 370 km) (Russell and Raymond, 2011). Here, we used the HAMO dataset with nominal spatial resolution of 360–400 m/pix.

The calibrated data (Filacchione and Ammannito, 2014) are cleaned for artifacts with the procedure described in Carrozzo et al. (2016). In order to analyze the spectral signature in the range of wavelengths affected by thermal emission (usually from 3.2 μm longward), we use the method described in Section 3 to remove the thermal emission. In this paper, photometric effects are corrected for both topographic variations and physical characteristics of the regolith using the Hapke approach (Ciarniello et al., 2017). However, other methods for photometric correction can be applied (Longobardo et al., 2017), yielding similar results, but they are not considered in this work.

To analyze a large dataset like the one considered in this work, we developed an automatic data process able to return different spectral indicators from Ceres observations. This algorithm allows us to map the spatial distribution of each spectral indicator across the surface (for more details about this algorithm, see Frigeri et al., 2017). The main spectral parameters selected are:

- photometrically corrected reflectance at 1.2 μm,
- spectral slope in the range 1.891–1.163 μm,
- band depths of phyllosilicate bands at 2.7,
- band depths of NH_4-phyllosilicate bands at 3.1 μm,
- band depths at 3.4 μm,

In the present work we also consider the band depths of carbonates at 3.3–3.5 μm, and 3.9 μm (not computed in the automatic algorithm).

3. Thermal removal

The observed spectra of Ceres' surface are affected by thermal emission from ~3.2 μm longward. The radiance of the thermal emission hides the absorption bands and prevents a comparison with laboratory data. We implemented a proper algorithm in order to remove the thermal emission while preserving the spectral features present in the spectra. This is made by modeling the total radiance as the sum of the solar radiance reflected by the surface and the thermal emission of the surface itself, and then performing the removal of the latter, as follows:

- The model of the solar reflected radiance is produced by a model of reflectance of the surface, multiplied by the solar irradiance at Ceres' heliocentric distance. To be consistent with the spectral modeling discussed in Section 5 we used the same reflectance model to estimate the reflectance level in the thermal emission range.
- The Planck function is summed up to this model in order to fit the total radiance level. Free parameters of the Planck function are temperature and emissivity. Their retrieved values are not discussed in the present work.
- Once the Planck function has been derived, we subtract it from the total measured radiance, and we divide the result by the solar irradiance to obtain the reflectance in the whole range.

The reflectance continuum in the thermal emission range, after removal of the Planck function, could be over or underestimated depending on the reflectance model used. However, the measured spectral features are not affected by this uncertainty. Typical result of thermal removal is shown in Fig. 2. The spectral range 3.3 – 4.2 μm, after thermal removal, present the absorption bands of the carbonates at 3.5 μm and 3.95 μm (see also Fig. 8).

4. Spectral analysis

The quadrangle is dominated by mostly highly degraded impact craters of diameters between 50 and 200 km and clusters of small to midsize impact craters. The seven most prominent impact craters have been named Coniraya, Gaue, Omonga, Ikapati, Achita, Ernutet, and Liber (see Fig. 1). Coniraya is the largest impact crater in the quadrangle, while Gaue and Ikapati craters are the freshest large impact craters. We refer to Pasckert et al. (2016) for a complete geological mapping of the Coniraya quadrangle.

Maps showing band parameters (Figs. 3–7) have been computed from VIR data acquired during the survey and HAMO phase.

We consider thermally corrected spectra as discussed in Section 3. Before producing the maps, the Hapke photometric correction has been applied to the VIR data (Hapke et al., 1993; Ciarniello et al., 2017). The maps have been corrected for roughness, single scattering phase function, and opposition effects using parameters derived by Ciarnello et al. (2017). The result of the correction procedure is the reflectance as observed in standard viewing geometry (incidence angle = 30°, emission angle = 0°). The methods used to produce the VIR data mosaic is fully described in

Please cite this article as: A. Raponi et al., Mineralogical mapping of Coniraya quadrangle of the dwarf planet Ceres, Icarus (2017), https://doi.org/10.1016/j.icarus.2017.10.023

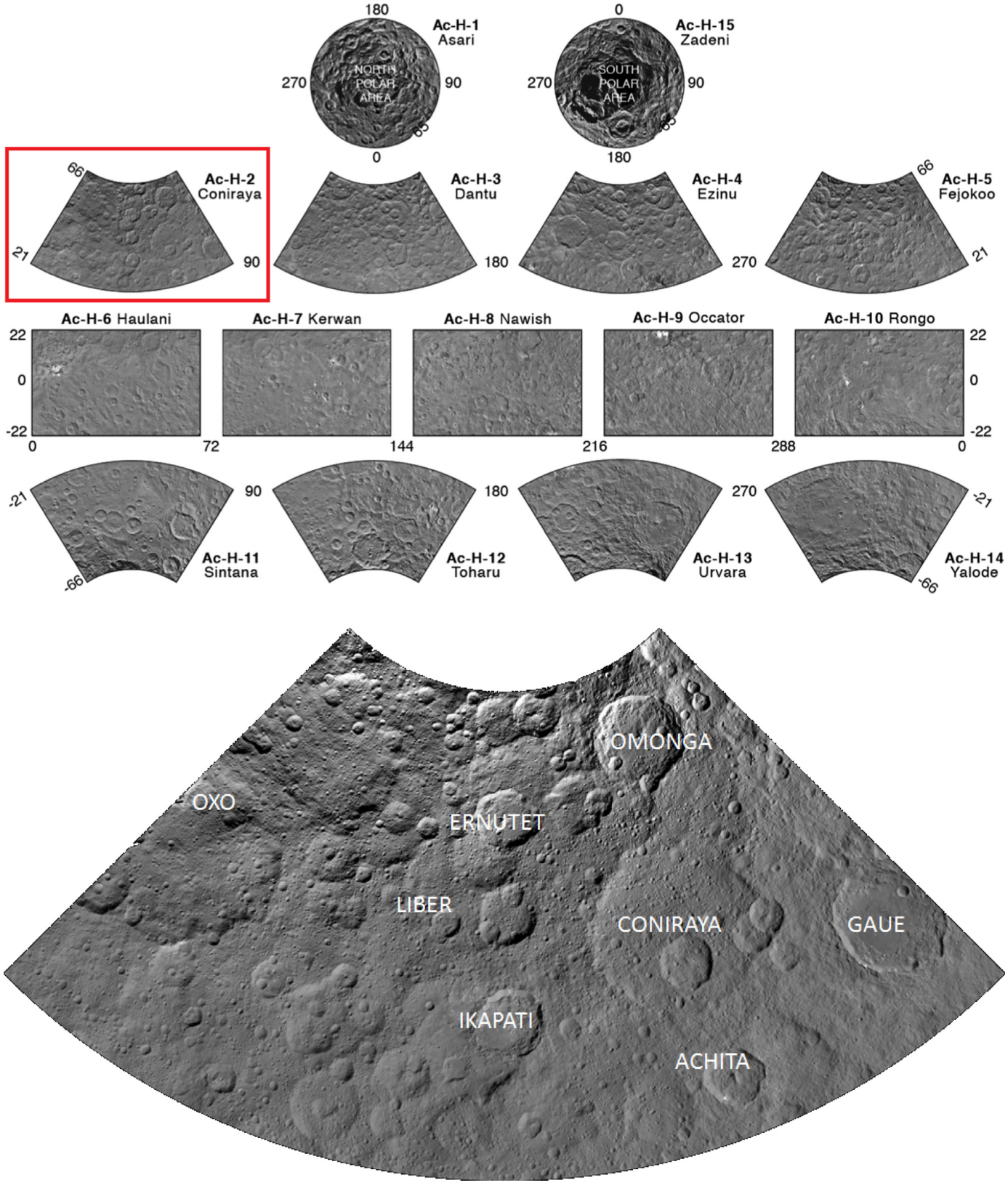

Fig. 1. Upper panel: figure adapted from Roatsch et al. (2016), showing the 15-quadrangle scheme in which Ceres' surface has been divided. The Coniraya quadrangle, highlighted in red, is the main focus of this study and is located at 0°–90°, 21°–66° N. Bottom: Dawn Framing Camera clear filter LAMO base map mosaic in the Lambert Conical projection, with 35 m/pixel resolution. The names of the main craters are indicated. (For interpretation of the references to color in this figure legend, the reader is referred to the web version of this article.)

Please cite this article as: A. Raponi et al., Mineralogical mapping of Coniraya quadrangle of the dwarf planet Ceres, Icarus (2017), https://doi.org/10.1016/j.icarus.2017.10.023

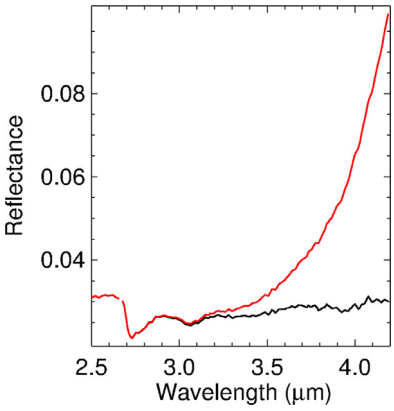

Fig. 2. Thermal emission removal of a typical spectrum of the average surface of Ceres. Red and black lines are respectively the reflectance spectra before and after thermal emission removal. (For interpretation of the references to color in this figure legend, the reader is referred to the web version of this article.).

Frigeri et al. (2017). The distribution of the 2.7 μm, 3.1 μm and 3.4 μm band depths are shown in Figs. 3–5. The corrected reflectance map at 1.2 μm is shown in Fig. 6, and the spectral slope is shown in Fig. 7.

According to De Sanctis et al. (2015); Ammannito et al. (2016); and De Sanctis et al. (2017), the band depth at 2.7 μm is correlated with Mg-phyllosilicate abundance, the 3.1 μm band depth is correlated with NH_4-phyllosilicate, and the 3.4-μm band depth in Ernutet is correlated with organic material abundance.

A global trend for the band depth at 2.7 μm (Fig. 3) shows a lower amount of phyllosilicates in crater floors and the crater's ejecta (see also Pasckert et al. (2016)), especially for the three central craters Ernutet, Liber, and Ikapati and for Gaue crater in the Eastern side of the quadrangle. The highest values for these end-members are found in the western, and southwestern sides of the map, where significant craters are not present.

The band depth at 3.1 μm has almost the same behavior of the 2.7-μm band depth (Fig. 4), apart from two considerations:

- the high latitudes present a systematic deeper band depth than the region at lower latitude;
- the Ernutet crater floor and surrounding terrains show an increase in band depth, differently from the 2.7-μm band depth and all the other large-sized craters.

The deep band depth at 3.4 μm in the Ernutet crater terrain (Fig. 5 and 7C) is an indication of a large abundance of organic aliphatic materials, as discussed in De Sanctis et al. (2017). It is the only case on the whole Ceres' surface where organics features are so evident.

The photometrically-corrected reflectance level at 1.2 μm returns a good correlation with the band depth at 3.4 μm (see Fig. 6). Moreover, the spectral slope appears redder in the Ernutet crater organic-rich areas (Figs. 7 and 8A). This would point to brighter albedo, and reddish spectra of the organic material than the average surface of Ceres.

Conversely, bluer spectra are detected in Ikapati floor and its crater ejecta (see Figs. 7, and 8A) pointing to differences in the composition as discussed in Sections 5 and 6.

We extract average spectra from three regions which appear to be the most peculiar within the quadrangle because of their differences with respect the average Ceres spectrum: Ernutet, Ikapati, and Gaue craters. In particular, carbonates absorptions of Ikapati are broader and shifted toward longer wavelengths with respect the other craters (Fig. 8). This is similar to the bright region in the Occator crater, where this shift has been attributed to a change in the carbonates composition, from Mg-Carbonate to Na-carbonates (De Sanctis et al., 2016). The Ikapati region shows Na-carbonates and could thus have been involved in processes similar to those suggested for the Occator crater, which include a recent aqueous alteration (De Sanctis et al., 2016). We refer to Carrozzo et al. (2017) for a complete discussion on the carbonate distribution on Ceres' surface.

5. Spectral modeling

To obtain an information on the abundances of the minerals making up the surface, we used a quantitative spectral analysis of the composition using Hapke's radiative transfer model (Hapke 1993, 2012) as described by Ciarniello et al. (2011) and Raponi et al. (2016). The whole formulation of the bidirectional reflectance (r) is:

$$r = \frac{SSA}{4\pi}\frac{\mu_0}{\mu + \mu_0}[B_{SH}p(g) + H(SSA,\mu)H(SSA,\mu_0) - 1] \times S(i,e,g,\theta)B_{CB} \quad (1)$$

Where i, e, g are the incidence, emission, and phase angles, respectively, and μ_0, μ are the cosines of the incidence and emission angles. These parameters come from the shape model and position of the spacecraft at the time of observation. The parameters that contain most of the spectral information are the single scattering albedo (SSA), and the related Ambartsumian–Chandrasekhar functions $H(SSA,\mu)$ describing the multiple scattering components.

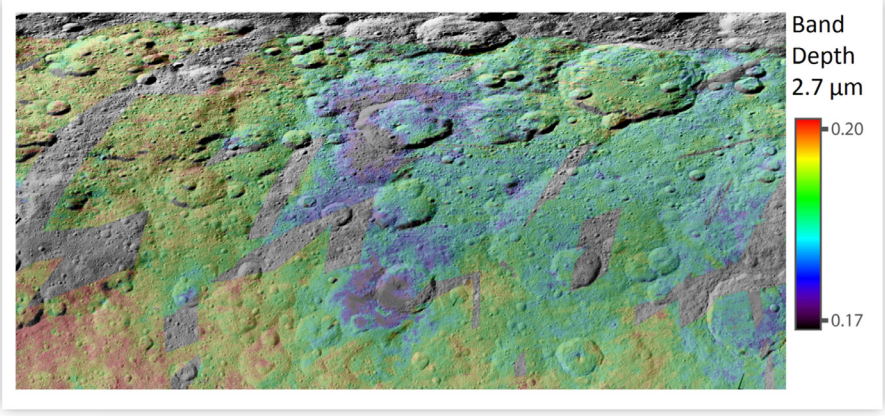

Fig. 3. The band depth at 2.7 μm shows the abundance of Mg-phyllosilicates.

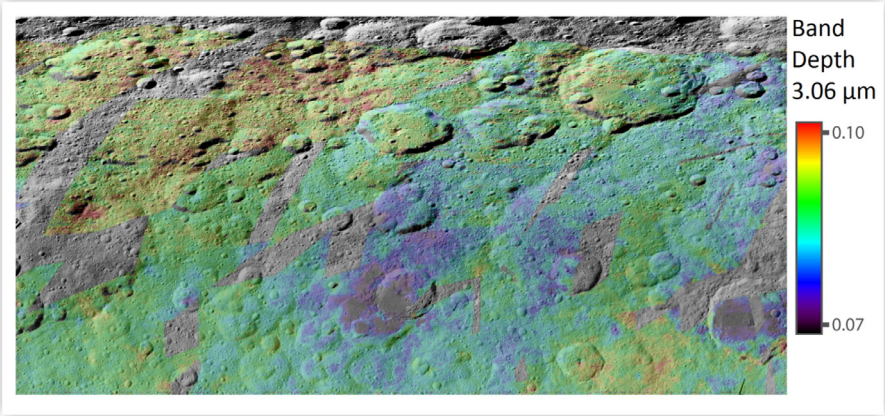

Fig. 4. The band depth at 3.1 µm is indicative of the NH4-phyllosilicates abundance.

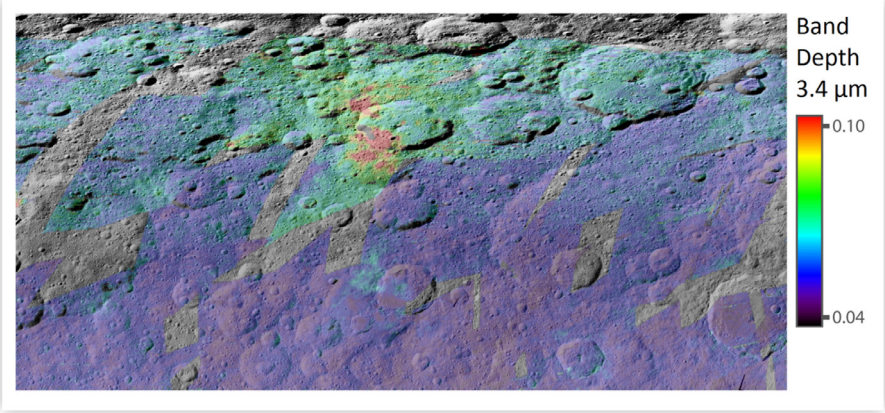

Fig. 5. The band depth at 3.4 µm is linked with the abundance of organic materials.

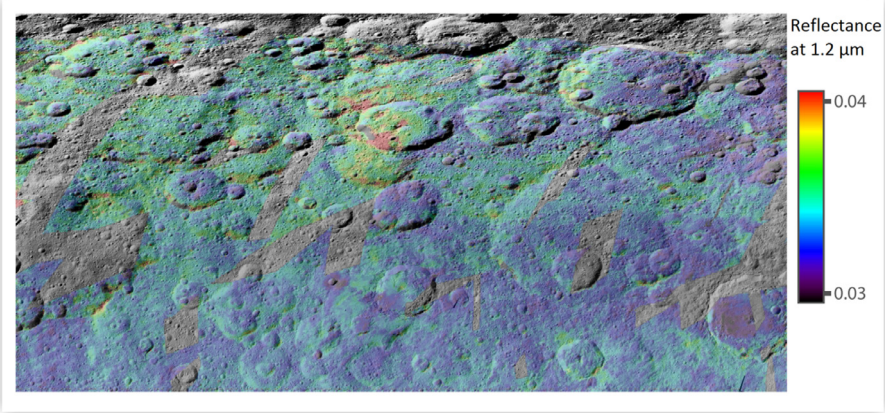

Fig. 6. Coniraya photometrically corrected reflectance map at 1.2 µm.

Other parameters describe the photometric behavior as a function of the viewing geometry, especially the phase function; they are:

- the single particle phase function $p(g)$,
- the shadow hiding opposition effect $B_{SH}(g)$,
- the coherent back-scattering opposition effect $B_{CB}(g)$,
- the shadow function modelling large-scale roughness $S(i, e, g, \theta)$, with θ being the average surface slope.

These photometric parameters are fixed after Ciarniello et al. (2017), who defined the average scattering properties of Ceres' regolith. The spectral properties are mainly affected by the SSA parameters. The latter have been modeled for an intimate mixing between different minerals, which implies that the particles of the end-member materials are in contact with each other and all are involved in the scattering of a single photon. The SSA of each mineral is defined starting from their grain size and their optical constants as described in Hapke (2012). The optical constants are derived from laboratory measurements (Table 1) with the method described by Carli et al. (2014).

The average SSA of the regolith is defined through the weights p, which represent the relative abundances of the minerals. The

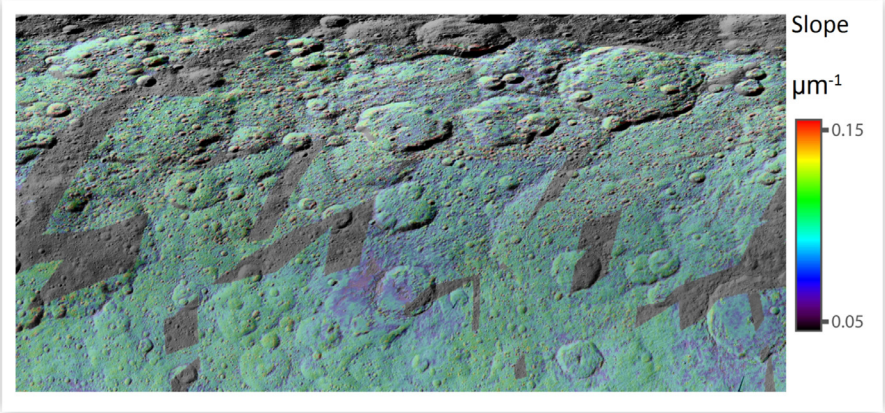

Fig. 7. Coniraya 1.891–1.163 μm spectral slope map. To calculate the spectral slope, we use the definition used by Filacchione et al. (2012): Slope = $(R_{\lambda 2}-R_{\lambda 1})/(\lambda 2-\lambda 1)/R_{\lambda 1}$, where $\lambda 1 = 1.163$ ν, $\lambda 2 = 1.891$ μm, and R_λ is the reflectance at λ.

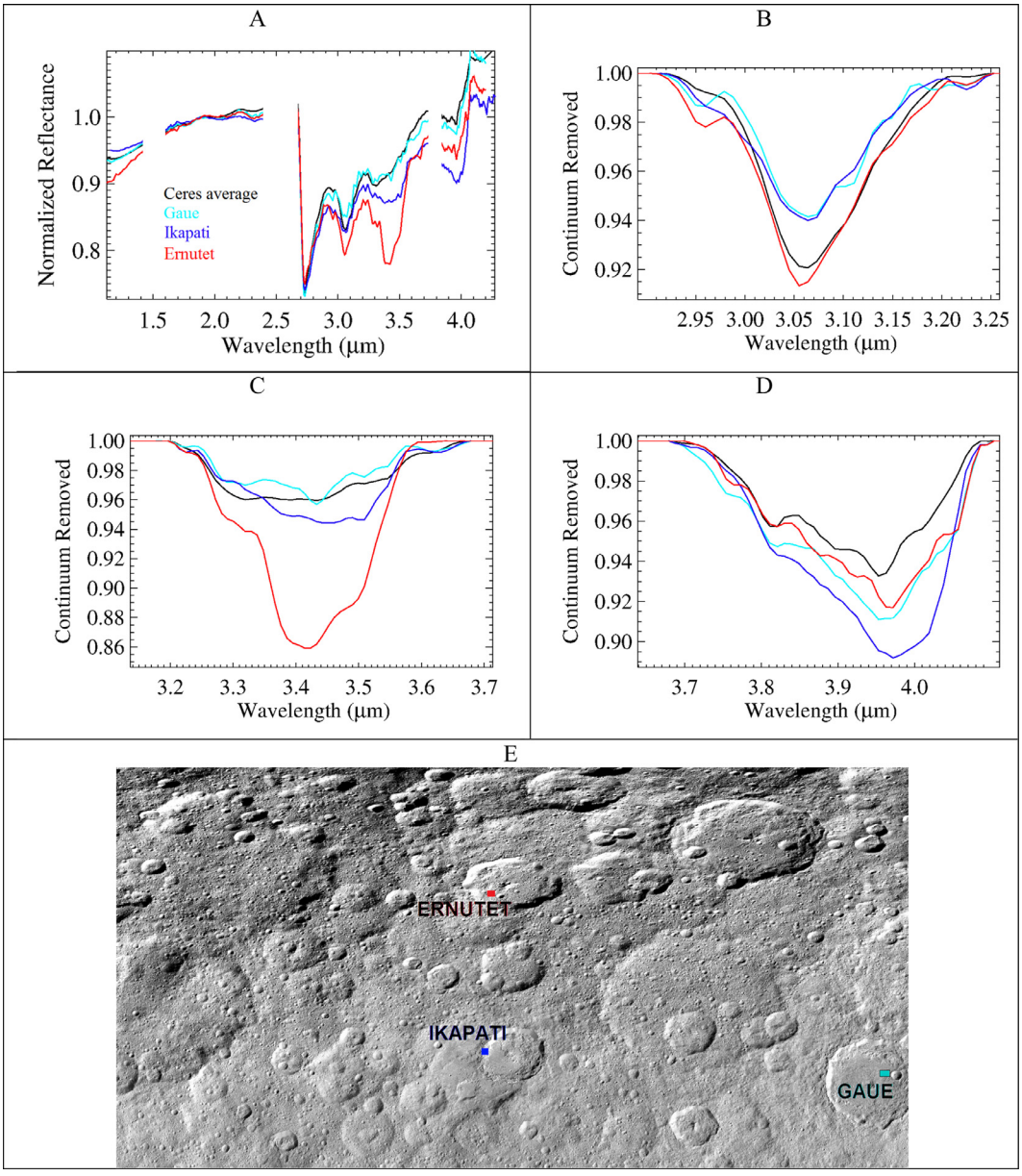

Fig. 8. Panel A: collected spectra normalized at 1.89 μm, from three different crater of Coniraya quadrangle, and the average Ceres spectrum (Ciarniello et al. 2017) for comparison. Panels B–D: spectral range centered on the main absorption bands, after smoothing and continuum removed. Each spectrum is an average of tens of pixel taken from the region indicated in Panel E.

Please cite this article as: A. Raponi et al., Mineralogical mapping of Coniraya quadrangle of the dwarf planet Ceres, Icarus (2017), https://doi.org/10.1016/j.icarus.2017.10.023

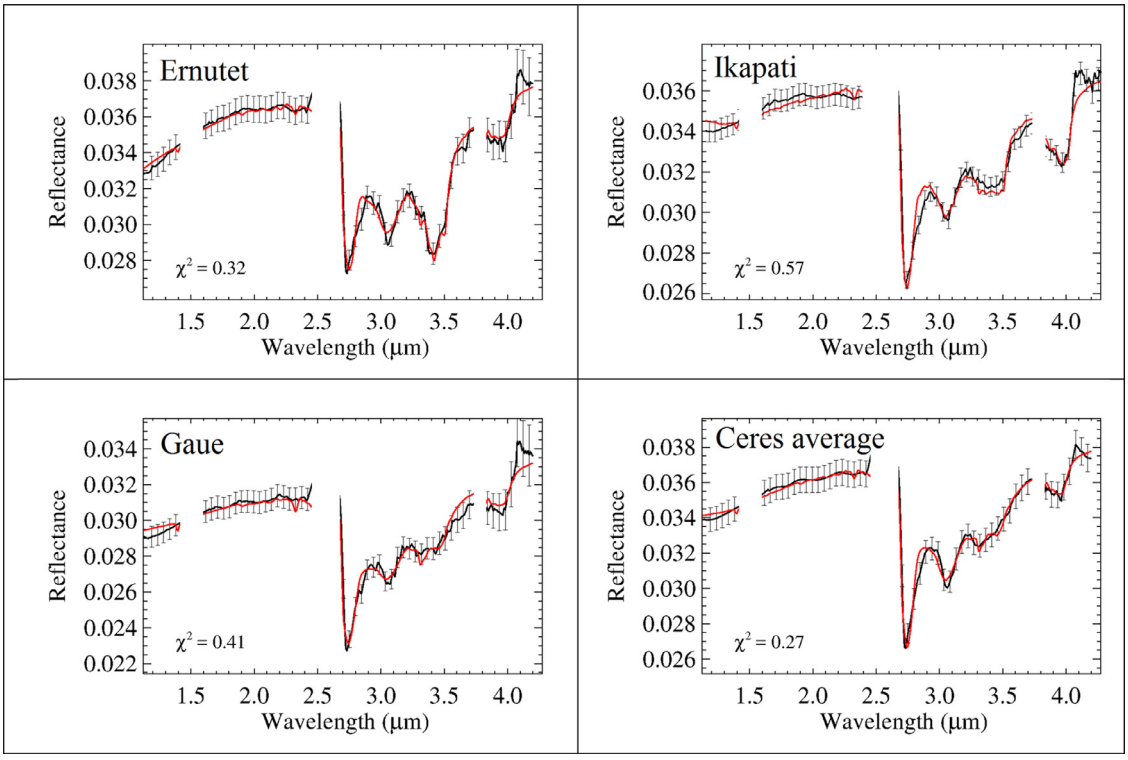

Fig. 9. Measured data with error bars of calibration uncertainties (black), and models (red), for the 4 average spectra shown in Fig. 8A. Retrieved parameters are shown in Table 2. (For interpretation of the references to color in this figure legend, the reader is referred to the web version of this article.)

Table 1
End-members used in calculating optical constants of the mineral types. Spectra are taken from the Relab spectral database.

Mineral	Type	Sample ID
Antigorite	Mg-phyllosilicate	AT-TXH-007
Dolomite	Mg-Ca-carbonate	CB-EAC-003
NH_4-montmorillonite	NH_4-phyllosilicate	JB-JLB-189
Magnetite	Dark material	MG-EAC-002
Heated Natrite	Na-carbonate	CB-EAC-034-C
Kerite	Organic-aliphatics	MA-ATB-043

weight p_i is defined as the cross section of the grains of the *i*th mineral as a fraction of the area. p is also a volume fraction, assuming grain sizes are equal for all minerals. Hereafter we refer to the weights p as "abundances".

$$SSA = SSA_1 p_1 + SSA_2 p_2 + SSA_3 p_3 + .. \quad \text{with} : p_1 + p_2 + p_3 + .. = 1 \tag{2}$$

The best-fitting result is obtained by comparison of the model with the measured spectra, applying the Levenberg–Marquardt method for non-linear least-squares multiple regression (Marquardt 1963).

Free model parameters to be retrieved are:

(i) abundances of the end-members;
(ii) grain size of the regolith (assumed equal for all end-members);
(iii) a multiplicative constant of the absolute level of reflectance of the model in order to account for uncertainties in the radiometric and photometric accuracies, as well as errors on the local geometry information due to unresolved shadows and roughness;
(iv) a slope added to the model in order to better fit the measured spectrum: in some cases, the measured spectra present an artificial slope where high signal contrast is measured between adjacent pixels, like regions near shadows. This is due to a varying spatial point spread function towards longer wavelengths (Filacchione 2006);
(v) temperature and effective emissivity (Davidsson et al., 2009). The latter is the product of the directional emissivity (Hapke 2012) and a free parameter used to account for unresolved shadow and the structure of the surface (Davidsson et al. 2009). Its interpretation is outside the scope of this work.

The total radiance is modeled by accounting for both the contributions of the reflected sunlight, and the thermal emission:

$$Rad = r \times \frac{F_\odot}{D^2} + \varepsilon_{eff} \times B(\lambda, T) \tag{3}$$

where r is the Hapke bidirectional reflectance (Eq. (1)), F_O is the solar irradiance at 1 AU, D is the heliocentric distance (in AU), ε_{eff} is the effective emissivity, $B(\lambda, T)$ is the Planck function. Thus, the estimation of the thermal emission discussed in Section 3 is done simultaneously with the reflectance modeling in order to yield a consistent result between these two contributions to the total signal measured.

The SSA is modeled starting from minerals already discussed in De Sanctis et al. (2015, 2016) (see Table 1) which are related to the average Ceres surface.

On Ceres' surface the predominant component is a dark material, whose identification is challenging, because its spectrum is featureless, except for the tentative absorption band centered at 1 μm, which can be attributed to iron (Fe). We found a good fit with magnetite (Fe_3O_4), however, a large amount of Fe is not consistent with GRAND measurements (Prettyman et al. 2017). More likely dark surface of Ceres should be composed by a large amount

Please cite this article as: A. Raponi et al., Mineralogical mapping of Coniraya quadrangle of the dwarf planet Ceres, Icarus (2017), https://doi.org/10.1016/j.icarus.2017.10.023

Table 2
Retrieved abundances from the best fits shown in Fig. 9. In all cases the rest of the composition is a dark neutral material as described in the text.

	Ernutet (%)	Ikapati (%)	Gaue (%)	Ceres average (%)
Mg-phyllosilicates	6.6	5.8	6.4	6.2
NH_4-phyllosilicates	7.5	3.3	3.8	7.0
Mg-Ca-carbonate	3.6	2.3	2.2	2.2
Na-carbonate	0.0	3.3	0.0	0.0
Organics	5.6	0.0	0.0	0.0

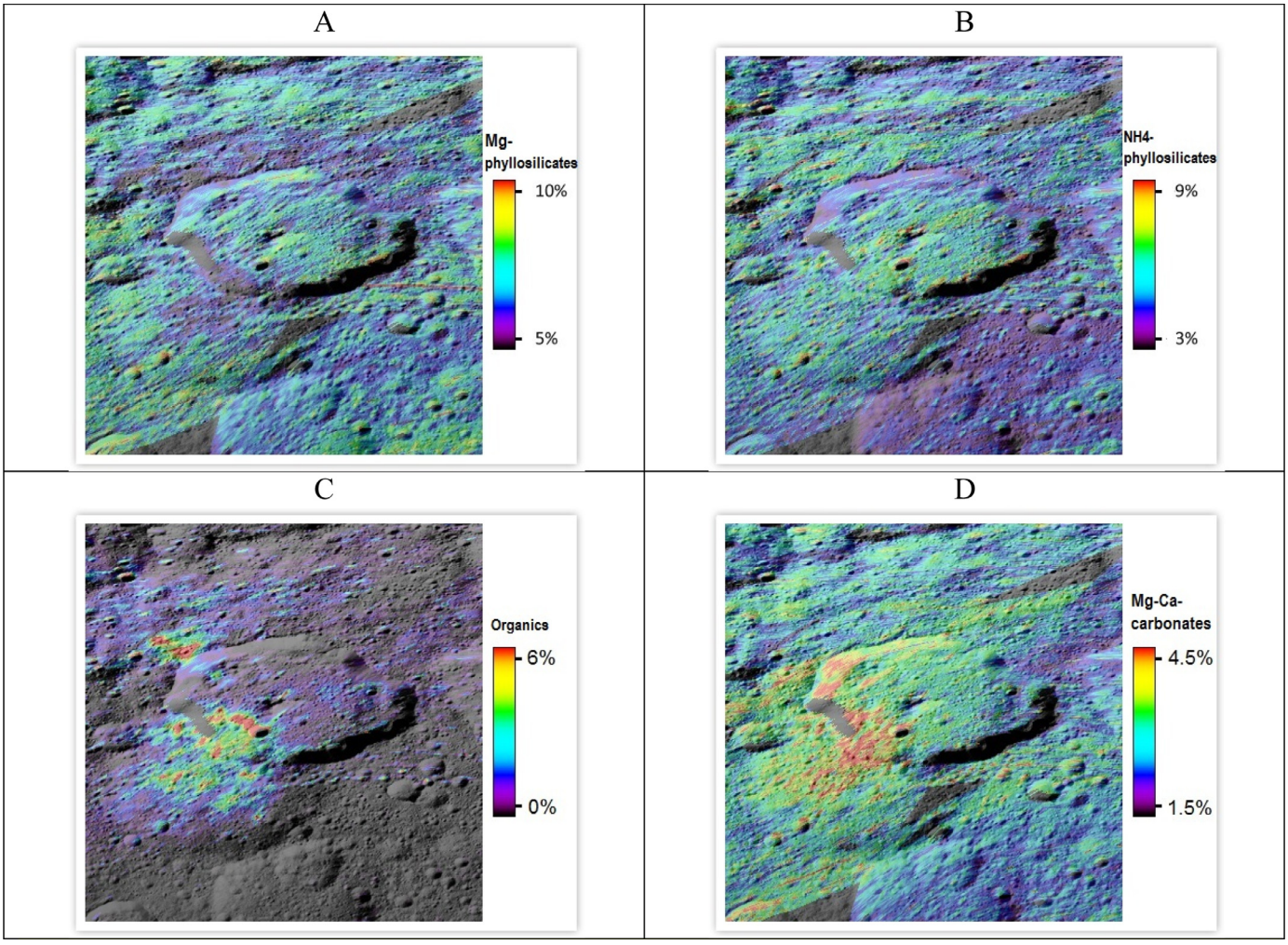

Fig. 10. Distributions of the abundances of the modeled endmembers of the Ernutet crater. Panel A: Mg-phyllosilicates, panel B: NH_4-phyllosilicate, panel C: organics, panel D: Mg–Ca-carbonates.

of carbon bearing material, being carbonaceous chondrite its close meteoritic analogue (Chapman and Salisbury, 1973, McSween et al., 2016). Moreover, we emphasize that the model used in this work is only based on spectral features, being the absolute signal level of the model adjusted with the multiplicative constant and the additional slope.

We apply the model to the average spectra of Ernutet, Ikapati and Gaue shown in Fig. 8, which turned out to be peculiar from the analysis of the quadrangle (previous section). The best fit are shown in Fig. 9, and the retrieved parameters in Table 2.

We also apply the spectral modeling to each pixel of the observations covering the whole area of the three craters. The abundances of the end members have been retrieved and projected (Figs. 10–12). The grain size retrieved was in all cases of the order of 100 µm, without clear variations on the maps. Thus we decided to fix this value in the fitting procedure.

5.1. Ernutet

Maps of Fig. 10C shows that abundance distribution of organics in Ernutet crater clearly define two regions with higher concentration:

- a larger region in the south-western rim with the higher concentration on the crater floor, but extending outside the crater
- a smaller region in the northern-western rim, located outside the crater floor.

With the resolution of the map (~400 m/px) we obtain a maximum concentration of 6%. However, we cannot exclude that non-resolved areas can contain more organics. The same consideration is valid for all the other abundances retrieved, and discussed hereafter. The rest of the surface appear to be devoid of organics. However, from the modeling we cannot exclude an amount < 1%.

Please cite this article as: A. Raponi et al., Mineralogical mapping of Coniraya quadrangle of the dwarf planet Ceres, Icarus (2017), https://doi.org/10.1016/j.icarus.2017.10.023

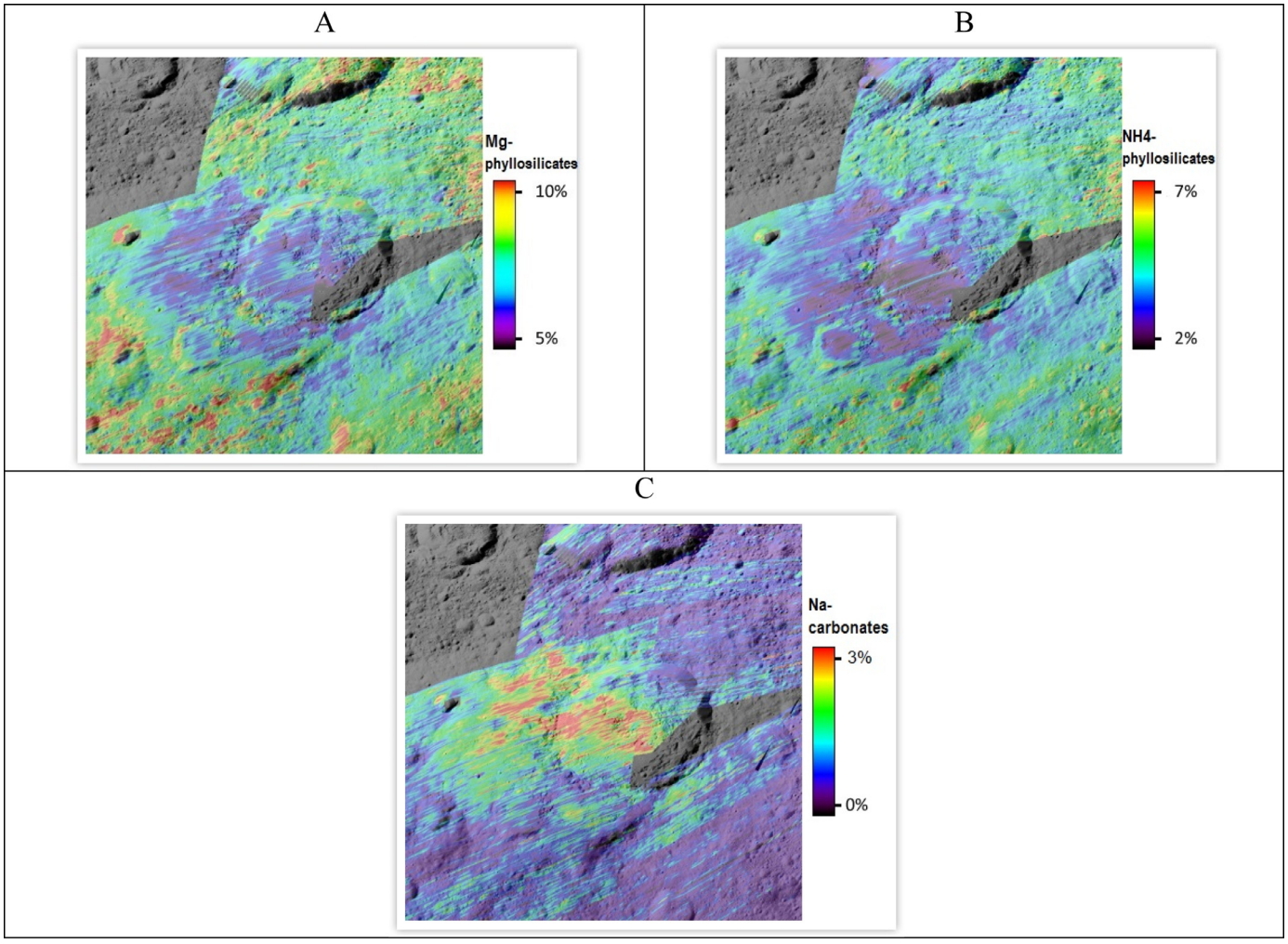

Fig. 11. Distributions of the abundances of the modeled endmembers of the Ikapati crater. Panel A: Mg-phyllosilicates, panel B: NH_4-phyllosilicate, panel C: Na-carbonates. Other end-members abundances are not shown because they do not present significant differences with respect the average surface.

Larger amount of Mg-phyllosilicates (Fig. 10A) is mapped inside the floor of Ernutet, up to 8–9%. The surrounding region of the rim are slightly depleted with respect the average Ceres surface. In particular the region with higher concentration of organics present a lower amount of Mg-phyllosilicates (5–6%).

Differently from the Mg-phyllosilicates, organic-rich regions contain larger amount of NH_4-phyllosilicates (up to 8–9% as shown in Fig. 10B). Eastern part of the map presents lower amount of NH_4-phyllosilicates (4–5%), while the floor of the crater has an heterogeneous amount.

Map of carbonates (Fig. 10D) shows an interesting correlation with the larger/southern organic-rich region. From modeling, carbonates are up to 4.5% in the southern part of the floor. The smaller/northern organic-rich region, does not present such a good correlation with carbonates.

5.2. Ikapati

Phyllosilicates maps of Ikapati crater shown in Fig. 11A and 11B, indicate a clear correlation between OH and NH_4 stretching in this crater. Lower amount has been found in the crater floor and in the western ejecta. In the same areas larger concentration of Na-carbonates has been derived from the model (up to 3%). Those carbonates are absent in the average Ceres surface, and only present in small specific areas (Palomba et al., 2017 submitted to Icarus), such as the faculae of the Occator crater.

5.3. Gaue

Differently from Ikapati crater, phyllosilicates maps of Gaue (Fig. 12A and 12B) are not well correlated each other: the map of Mg-phyllosilicates has an heterogeneous distribution with values ranging from 5 to 10%, while the map of NH_4-phyllosilicate clearly presents a lower amount on the crater floor (2–3%), and about 6% outside it. However, the two end-member are well correlated in a small region in the north/western part of the map, were larger amount of both Mg and NH_4-phyllosilicates have been derived: respectively 10% and 7%.

6. Discussion and conclusions

From the analysis of the Coniraya quadrangle, some relevant characteristics emerge. Here we discuss the major findings in the general context of Ceres' surface.

6.1. Phyllosilicates distribution

The band depth at 2.7 and 3.1 μm mapped in this work are both indicative of phyllosilicate abundance, and relative differences in their distributions are detectable (e.g., between Ikapati and Gaue craters). This was also highlighted by Ammannito et al. (2016) as a general result for Ceres' surface.

Please cite this article as: A. Raponi et al., Mineralogical mapping of Coniraya quadrangle of the dwarf planet Ceres, Icarus (2017), https://doi.org/10.1016/j.icarus.2017.10.023

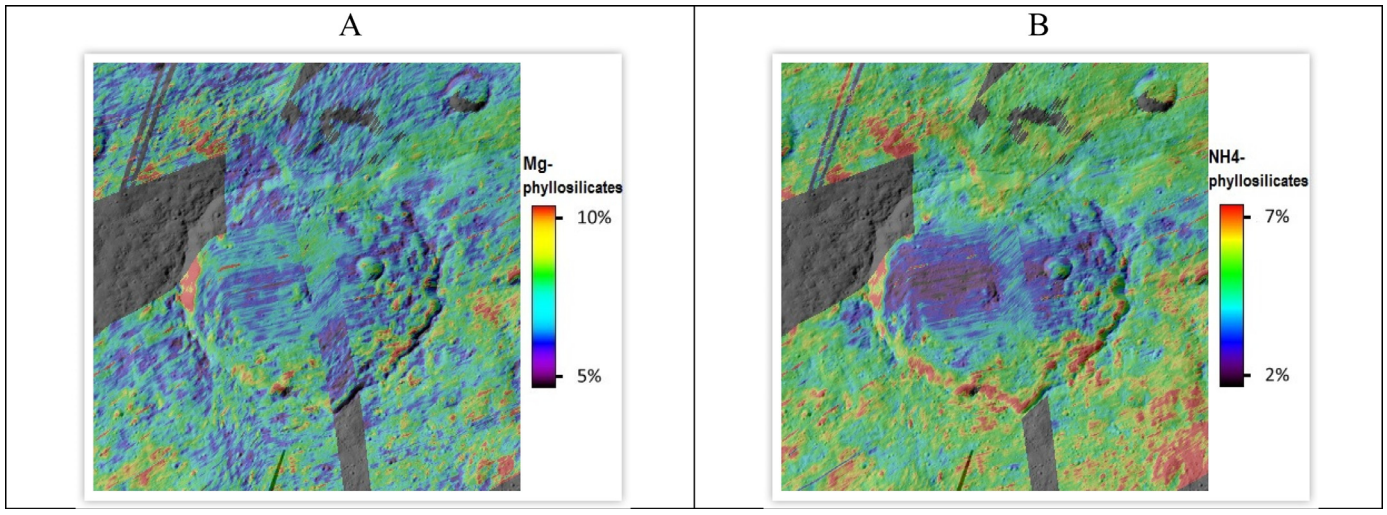

Fig. 12. Gaue crater. Mg-phyllosilicates and NH_4-phyllosilicate abundances. Other parameters are not shown because they do not present significant differences with respect the average surface.

The floor of the freshest and largest craters present smaller band depth at 2.7 and 3.1 μm.

The modeling performed for Ernutet, Ikapati, and Gaue craters reveals that the smaller band depth can be interpreted as a lower amount of Mg/NH_4-phyllosilicates. Smaller phyllosilicates band associates with relatively young crater seems quite common on Ceres' surface (De Sanctis et al. 2017), which may be the result of a volatile depletion due to impact heating. A noticeable exception is represented by the large-scale depression of Vendimia Planitia, located in the eastern adjacent quadrangles. The measured phyllosilicate absorptions at 2.7 and 3.1 μm, in two main craters located in this area, Dantu (Stephan et al., 2017) and Kerwan (Palomba et al., 2017), are stronger than its surrounding areas, and they actually are the deepest phyllosilicate absorptions measured on Ceres (Stephan et al., 2017). This observed trend may reveal a change in the composition of Ceres' crust with increasing depth below the topographic mean (Stephan et al., 2017).

The Mg and NH_4-phyllosilicates modeled present different depletion in the three craters mapped in Figs. 10–12. The cases that stand out are the high contrast for Ikapati crater floor and ejecta (Fig. 11A, 11B), and the NH_4-phyllosilicates on the Gaue crater floor (Fig. 12B).

This would point to a complex picture in which different processes can concur to determine the volatiles abundances during the impact (e.g., energy released by the impactor, depth of excavation), after the impact (e.g., aqueous alteration, hydrothermal activity, lateral mixing by micrometeoritic impacts, space weather), and could also reflect heterogeneities on Ceres' surface preexistent to the impact event.

6.2. Ikapati crater and ejecta

As discussed in the previous section, Ikapati fresh crater shows slightly smaller band depth at 2.7 and 3.1 μm, which would mean a lower concentration of Mg/NH_4-phyllosilicates. By taking into account the average spectrum shown in Fig. 10, we notice other relevant differences: larger absorption band of carbonates, and bluer spectral slope. Moreover, the band center of the carbonates absorption band shows a shift from 3.95 to 4.0 μm (see Fig. 8D), similar to the bright region in the Occator crater, where this shift has been attributed to a change in the carbonates composition, from Mg-Carbonate to Na-Carbonates (De Sanctis et al., 2016). The Ikapati region could thus have been involved in similar processes, as suggested for the Occator crater, which include a recent aqueous alteration (De Sanctis et al., 2016). However, in Ikapati the Na-carbonate is spread in the floor and ejecta, rather than being concentrated in specific regions inside the crater floor. This can be the result of the impact event of Ikapati that spread bright material previously concentrated in faculae like in Occator crater. This hypothesis would point to a unique formation process for all bright material present on the surface as suggested by (Stein et al., 2017), being their differences due to the following story of impact events.

Contrarily to the slow process occurring to form the bright material, the volatile depletion due to the impact induced heating could be fast, and it can explain the correlation of the lower amount of hydrated (OH- stretching) and ammoniated phyllosilicates (NH_4-strecthing) in correspondence of the ejecta.

6.3. Ernutet crater and organic-rich regions

The Ernutet crater is a unique feature of Ceres' surface, revealing a large amount of organic material that is mapped in this work by the 3.4-μm absorption band, and the abundance map of Fig. 10C. This absorptions is characteristic of the symmetric and antisymmetric stretching frequencies of methyl (CH_3) and methylene (CH_2) functional groups, typical of aliphatic hydrocarbons (Orthous-Daunay et al., 2013). The model performed in the present work (Fig. 9A) and in (De Sanctis et al. 2016) shows that Ceres organics signatures are very similar with the organic bands of terrestrial hydrocarbons such as kerite.

An evident correlation with organics distribution has been found with the absolute level of reflectance at 1.2 μm (Fig. 6), and the reddish slope (Fig. 7), revealing a possible constraint on the optical properties of the organic material: brighter and more reddish than the average surface of Ceres.

The abundance map of organics shown in Fig. 10C clearly define two regions with higher concentration of organics. In the work of De Sanctis et al. (2016) these two regions were labeled as region A (southern) and B (northern). In the same two regions we derived:

(1) smaller abundance of Mg-phyllosilicates (Fig. 10A);
(2) slightly larger abundance of NH_4-phyllosilicates (Fig. 10B);
(3) only in the southern region larger abundance of Mg-Ca-carbonates (Fig. 10D).

De Sanctis et al. 2016 suggested an endogenous origin of the organics, on the base of the larger presence of carbonates, (and slight larger presence of NH_4-phyllosilicates), both being products

of an hydrothermal activity together with the organics. An exogenous origin would require further explanations about the correlation with minerals (carbonates, NH_4-phyllosilicates) extensively present on Ceres surface, but unseen in the asteroid belt with the same amount.

The uniqueness of such organic-rich region would point to an uncommon condition over Ceres' surface. However, the asymmetry of the retrieved parameters in the two regions (point 3), would point to formation processes under different thermophysical and/or chemical conditions, occurring very close each other, but both favorable for the organics formation.

Further efforts are needed to assess the mechanism responsible for the formation and transport to the surface of minerals which should have a different origin with respect the common Ceres minerals, like organics and Na-carbonates.

The uniqueness of specific places on Ceres surface, together with the diversity of mineralogy is an indication of a complex environment typical of an active body.

Acknowledgments

VIR is funded by the Italian Space Agency-ASI and was developed under the leadership of INAF-Istituto di Astrofisica e Planetologia Spaziali, Rome-Italy. The instrument was built by Selex-Galileo, Florence-Italy. The authors acknowledge the support of the Dawn Science, Instrument, and Operations Teams. This work was supported by ASI-INAF n. I/004/12/0 and NASA.

References

Ammannito, E., De Sanctis, M.C., Ciarniello, M., Frigeri, A., Carrozzo, F.G., Combe, J.-Ph., Ehlmann, B.L., Marchi, S., McSween, H.Y., Raponi, A., Toplis, M.J., Tosi, F., Castillo-Rogez, J.C., Capaccioni, F., Capria, M.T., Fonte, S., Giardino, M., Jaumann, R., Longobardo, A., Joy, S.P., Magni, G., McCord, T.B., McFadden, L.A., Palomba, E., Pieters, C.M., Polanskey, C.A., Rayman, M.D., Raymond, C.A., Schenk, P.M., Zambon, F., Russell, C.T., 2016. Distribution of phyllosilicates on the surface of Ceres. Science 353 (6303). doi:10.1126/science.aaf4279, id.aaf4279.

Carrozzo, F.G., Raponi, A., De Sanctis, M.C., Ammannito, E., Giardino, M., D'Aversa, E., Fonte, S., Tosi, F., 2016. Artifacts reduction in VIR/Dawn data. Rev. Sci. Instrum. 87 (12). doi:10.1063/1.4972256, id.124501.

Carli, C., Ciarniello, M., Capaccioni, F., Serventi, G., Sgavetti, M., 2014. Spectral variability of plagioclase-mafic mixtures (2): Investigation of the optical constant and retrieved mineral abundance dependence on particle size distribution. Icarus 235, 207–219.

Carrozzo, F.G., De Sanctis, M.C., Raponi, A., Ammannito, E., Castillo-Rogez, J.C., Ehlmann, B.L., Marchi, S., Stein, N., Ciarniello, M., Tosi, F., Capaccioni, F., Capria, M.T., Fonte, S., Formisano, M., Frigeri, A., Giardino, M., Longobardo, A., Magni, G., Palomba, E., Zambon, F., Raymond, C.A., Russell, C.T., 2017. Nature, formation and distribution of carbonates on Ceres. Science. (Forthcoming).

Chapman, C.R., Salisbury, J.W., 1973. Comparisons of meteorite and asteroid spectral reflectivities. Icarus 19, 507–522.

Ciarniello, M., Capaccioni, F., Filacchione, G., Clark, R.N., Cruikshank, D.P., Cerroni, P., Coradini, A., Brown, R.H., Buratti, B.J., Tosi, F., Stephan, K., 2011. Hapke modeling of Rhea surface properties through Cassini-VIMS spectra. Icarus 214, 541–555.

Ciarniello, M., De Sanctis, M.C., Ammannito, E., Raponi, A., Longobardo, A., Palomba, E., Carrozzo, F.G., Tosi, F., Li, J.-Y., Schröder, S.E., Zambon, F., Frigeri, A., Fonte, S., Giardino, M., Pieters, C.M., Raymond, C.A., Russell, C.T., 2017. Spectrophotometric properties of dwarf planet Ceres from the VIR spectrometer on board the Dawn mission. Astron. Astrophys. 598. doi:10.1051/0004-6361/201629490, id.A130.

Combe, J.-Ph., McCord, T.B., Tosi, F., Ammannito, E., Carrozzo, F.G., De Sanctis, M.C., Raponi, A., Byrne, S., Landis, M.E., Hughson, K.H.G., Raymond, C.A., Russell, C.T., 2016. Detection of local H_2O exposed at the surface of Ceres. Science 353 (6303). doi:10.1126/science.aaf3010, id.aaf3010.

Combe, J.-Ph., Raponi, A., Tosi, F., De Sanctis, M.C., Carrozzo, F.G., Zambon, F., Ammannito, E., Hughson, K.H.G., Nathues, A., Hoffmann, M., Platz, T., Thangjam, G., Schorghofer, N., Schröder, S.E., Byrne, S., Landis, M.E., Ruesch, O., McCord, T.B., Johnson, K.E., Singh, S.M., Raymond, C.A., Russell, C.T., 2017. Exposed H2O-rich areas detected on Ceres with the Dawn Visible and InfraRed mapping spectrometer. Icarus. (Forthcoming).

Davidsson, Björn J.R., Gutiérrez, Pedro J., Rickman, Hans, 2009. Physical properties of morphological units on Comet 9P/Tempel 1 derived from near-IR Deep Impact spectra. Icarus 201, 335–357.

De Sanctis, M.C., Coradini, A., Ammannito, E., Filacchione, G., Capria, M.T., Fonte, S., Magni, G., Barbis, A., Bini, A., Dami, M., Ficai-Veltroni, I., Preti, G.the VIR Team, 2011. The VIR spectrometer. Space Sci. Rev. 163 (1–4), 329–369. doi:10.1007/s11214-010-9668-5.

De Sanctis, M.C., Ammannito, E., Raponi, A., Marchi, S., McCord, T.B., McSween, H.Y., Capaccioni, F., Capria, M.T., Carrozzo, F.G., Ciarniello, M., Longobardo, A., Tosi, F., Fonte, S., Formisano, M., Frigeri, A., Giardino, M., Magni, G., Palomba, E., Turrini, D., Zambon, F., Combe, J.-Ph., Feldman, W., Jaumann, R., McFadden, L.A., Pieters, C.M., Prettyman, T., Toplis, M., Raymond, C.A., Russell, C.T., 2015. Ammoniated phyllosilicates with a likely outer Solar System origin on (1) Ceres. Nature 528 (7581), 241–244. doi:10.1038/nature16172.

De Sanctis, M.C., Raponi, A., Ammannito, E., Ciarniello, M., Toplis, M.J., McSween, H.Y., Castillo-Rogez, J.C., Ehlmann, B.L., Carrozzo, F.G., Marchi, S., Tosi, F., Zambon, F., Capaccioni, F., Capria, M.T., Fonte, S., Formisano, M., Frigeri, A., Giardino, M., Longobardo, A., Magni, G., Palomba, E., McFadden, L.A., Pieters, C.M., Jaumann, R., Schenk, P., Mugnuolo, R., Raymond, C.A., Russell, C.T., 2016. Bright carbonate deposits as evidence of aqueous alteration on (1) Ceres. Nature 536 (7614), 54–57. doi:10.1038/nature18290.

De Sanctis, M.C., Ammannito, E., McSween, H.Y., Raponi, A., Marchi, S., Capaccioni, F., Capria, M.T., Carrozzo, F.G., Ciarniello, M., Fonte, S., Formisano, M., Frigeri, A., Giardino, M., Longobardo, A., Magni, G., McFadden, L.A., Palomba, E., Pieters, C.M., Tosi, F., Zambon, F., Raymond, C.A., Russell, C.T., 2017. Localized aliphatic organic material on the surface of Ceres. Science 355 (6326), 719–722. doi:10.1126/science.aaj2305.

Filacchione, G., 2006. Calibrazioni a terra e prestazioni in volo di spettrometri ad immagine nel visibile e nel vicino infrarosso per l'esplorazione planetaria. Ph.D thesis. Università di Napoli Federico II, 316 pages.

Filacchione, G., Ammannito, E. Dawn VIR Calibration Document, version 2.4 (2014), https://sbn.psi.edu/archive/dawn/vir/DWNVVIR_I1B/DOCUMENT/VIR_CALIBRATION/VIR_CALIBRATION_V2_4.PDF.

Filacchione, G., Capaccioni, F., Ciarniello, M., Clark, R.N., Cuzzi, J.N., Nicholson, P.D., Cruikshank, D.P., Hedman, M.M., Buratti, B.J., Lunine, J.I., Soderblom, L.A., Tosi, F., Cerroni, P., Brown, R.H., McCord, T.B., Jaumann, R., Stephan, K., Baines, K.H., Flamini, E., 2012. Saturn's icy satellites and rings investigated by Cassini-VIMS: III - Radial compositional variability. Icarus 220 (2), 1064–1096.

Frigeri, A. De Sanctis, M.C., Ammannito, E., Tosi, F., Ciarniello, M., Zambon, F., Carrozzo, F.G., Raponi, A., McCord, T.B., Raymond, C.A., Russell, C.T., 2017. The spectral parameter maps of Ceres from NASA/DAWN VIR data. Icarus. (Forthcoming).

Hapke, B., 1993. Theory of Reflectance and Emittance Spectroscopy. Cambridge University Press.

Hapke, B., 2012. Theory of Reflectance and Emittance Spectroscopy, second ed. Cambridge University Press.

Konopliv, A.S., Asmar, S.W., Bills, B.G., Mastrodemos, N., Park, R.S., Raymond, C.A., Smith, D.E., Zuber, M.T., 2011. The Dawn gravity investigation at Vesta and Ceres. Space Sci. Rev. 163, 461–486.

Longobardo, A., et al., 2017. Mineralogy of the Occator quadrangle. Icarus, (Forthcoming).

Marquardt, D., 1963. SIAM. J. Appl. Math. 11, 431.

McSween, H.Y., Castillo-Rogez, J., Emery, J.P., De Sanctis, M.C., Dawn Science Team Rationalizing the Composition and Alteration of Ceres, 47th Lunar and Planetary Science Conference, held March 21–25, 2016 at The Woodlands, Texas. LPI Contribution No. 1903, p.1258 (2016).

Orthous-Daunay, F.-R., Quirico, E., Beck, P., Brissaud, O., Dartois, E., Pino, T., Schmitt, B., 2013. Mid-infrared study of the molecular structure variability of insoluble organic matter from primitive chondrites. Icarus 223, 534–543.

Palomba, E., Longobardo, A., De Sanctis, M.C., Carrozzo, F.G., Galiano, A., Zambon, F., Raponi, A., Ciarniello, M., Stephan, K., Williams, D., Ammannito, E., Capria, M.T., Fonte, S., Giardino, M., Tosi, F., Raymond, C.A., Russell, C.T., 2017. Mineralogical mapping of the Kerwan quadrangle on Ceres. Icarus. (Forthcoming).

Pasckert, J.H., Hiesinger, H., Williams, D.A., Crown, D.A., Mest, S.C., Buczkowski, D.L., Scully, J.E.C., Schmedemann, N., Jaumann, R., Roatsch, T., Preusker, F., Nass, A., Nathues, A., Hoffmann, M., Schäfer, M., De Sanctis, M.C., Raymond, C.A., Russell, C.T., 2016. Geologic mapping of the Ac-H-2 coniraya quadrangle of Ceres from NASA's dawn mission. In: Proceedings of the Forty-Seventh Lunar and Planetary Science Conference, LPI Contribution No. 1903, p. 1450.

Prettyman, T.H., Feldman, W.C., McSween, H.Y., Dingler, R.D., Enemark, DonaldC., Patrick, D.E., Storms, S.A., Hendricks, JohnS., Morgenthaler, J.P., Pitman, K.M., Reedy, R.C., 2011. Dawn's gamma ray and neutron detector. Space Sci. Rev. 163, 371–459.

Raponi, A., Ciarniello, M., Capaccioni, F., Filacchione, G., Tosi, F., De Sanctis, M.C., Capria, M.T., Barucci, M.A., Longobardo, A., Palomba, E., Kappel, D., Arnold, G., Mottola, S., Rousseau, B., Rinaldi, G., Erard, S., Bockelee-Morvan, D., Leyrat, C., 2016. The temporal evolution of exposed water ice-rich areas on the surface of 67P/Churyumov–Gerasimenko: spectral analysis. MNRAS 462.

Raponi, A., De Sanctis, M.C., Carrozzo, F.G., Ciarniello, M., Castillo-Rogez, J.C., Ammannito, E., Frigeri, A., Longobardo, A., Palomba, E., Tosi, F., Zambon, F., Raymond, C.A., Russell, C.T., 2017. Mineralogy of Occator Crater on Ceres. In press.

Roatsch, T., Kersten, E., Matz, K.-D., Preusker, F., Scholten, F., Jaumann, R., Raymond, C.A., Russell, C.T., 2016. High-resolution Ceres high altitude mapping orbit atlas derived from dawn framing camera images. Planet. Space Sci. 129, 103–107. doi:10.1016/j.pss.2016.05.011.

Russell, C.T., Raymond, C.A., 2011. The dawn mission to Vesta and Ceres. Space Sci. Rev. 163, 3–23.

Sierks, H., Keller, H.U., Jaumann, R., Michalik, H., Behnke, T., Bubenhagen, F., Büttner, I., Carsenty, U., Christensen, U., Enge, R., Fiethe, B., Gutiérrez-Marqués, P., Hartwig, H., Krüger, H., Kühne, W., Maue, T., Mottola, S., Nathues, A., Reiche, K.-U., Richards, M.L., Roatsch, T., Schröder, S.E., Szemerey, I., Tschentscher, M., 2011. The dawn framing camera. Space Sci. Rev. 163 (1–4), 263–327. doi:10.1007/s11214-011-9745-4.

Singh, S., Combe, J.-Ph., McFadden, L.A., McCord, T.B., Johnson, K.E., Hughson, K.H.G., Zambon, F., Ciarniello, M., Carrozzo, F.G., Ammannito, E., De Sanctis, M.C., Ruesch, O., Stephan, K., Tosi, F., Longobardo, A., Raymond, C.A., Russell, C.T., 2017. Mineralogy mapping of the Ac-H-5 Fejokoo quadrangle of Ceres. Icarus (Forthcoming).

Stein, N., Ehlmann, B.L., Palomba, E., De Sanctis, M.C., Nathues, A., Hiesinger, H., Ammannito, E., Raymond, C.A., Jaumann, R., Longobardo, A., Russell, C.T., 2017. The formation and evolution of bright spots on Ceres, Icarus. (Forthcoming).

Stephan, K., Jaumann, R., Zambon, F., Carrozzo, F.G., De Sanctis, M.C., Tosi, F., Ammannito, E., Longobardo, A., Palomba, E., McFadden, L.A., Krohn, K., Williams, D.A., Raponi, A., Ciarniello, M., Combe, J.-Ph., Frigeri, A., Roatsch, T., Matz, K.-D., Preusker, F., Raymond, C.A., Russell, C.T., 2017b. Spectral investigation of quadrangle Ac-H-3 of the dwarf planet Ceres – the region of impact crater Dantu. Icarus (Forthcoming).

Please cite this article as: A. Raponi et al., Mineralogical mapping of Coniraya quadrangle of the dwarf planet Ceres, Icarus (2017), https://doi.org/10.1016/j.icarus.2017.10.023